RSC Advances

PAPER

View Article Online
View Journal | View Issue

Cite this: *RSC Adv.*, 2017, **7**, 32607

Influence of Mn dopants on the electrical properties of $Pb(In_{0.5}Nb_{0.5})O_3$–$PbTiO_3$ ferroelectric single crystals

Huimin Qiao,[ab] Chao He,*[a] Zujian Wang,[a] Dongfang Pang,[a] Xiuzhi Li,[a] Ying Liu[a] and Xifa Long*[a]

Received 6th May 2017
Accepted 1st June 2017

DOI: 10.1039/c7ra05102f

rsc.li/rsc-advances

In order to study the influence of Mn doping on the electrical properties of PIN–PT single crystals and develop the materials for high power applications, relaxor-based $0.68Pb(In_{0.5}Nb_{0.5})O_3$–$0.32Pb(Ti_{0.92}Mn_{0.08})O_3$ (Mn-PIN–PT) ferroelectric single crystals with pseudo-cubic symmetry were grown *via* the conventional flux method. The Mn-PIN–PT crystals have a Curie temperature (T_C) of 231 °C and ferroelectric phase transition (T_{MPB}) of 175 °C. Relaxor behavior is identified by the frequency dispersion in dielectric spectra. The piezoelectric coefficient and longitudinal electromechanical coupling factor (k_{33}) are 730 pC N^{-1} and 80% at room temperature, respectively. The temperature coefficient of k_{33} is 1.6%, showing good stability up to 180 °C. The ferroelectric properties were measured at different electric fields, showing well-shaped hysteresis loops above 20 kV cm^{-1}. The variation of remnant polarization (P_r), coercive field (E_C) and internal bias field (E_i) as a function of temperature was investigated. The Curie temperature and ferroelectric phase transition temperature were decreased and increased, respectively, due to Mn doping, and a typical hard doping effect was confirmed *via* ferroelectric, dielectric and piezoelectric characterization.

1. Introduction

The binary relaxor-based ferroelectric solid solutions with a formula of $(1-x)Pb(B_1,B_2)O_3$–$PbTiO_3$ ($B_1 = Mg^{2+}$, Yb^{3+}, Zn^{2+}, In^{3+}, Sc^{3+}…, $B_2 = Nb^{5+}$, Ta^{5+}…) have drawn much attention in recent years for their outstanding electrical, electromechanical and pyroelectric properties, making them promising candidates for non-destructive testing, wireless communication and medical ultrasonic imaging.[1,2] However, the features of low coercive field, low mechanical quality factor ($Q_m < 100$) and inferior thermal stability have restricted their applications in various fields.[3,4] In recent years, much attention has been drawn to the modification of relaxor-PT solid solutions by chemical additions, particularly by Fe and Mn substitutions.[5,6] As is known to us, the Mn ions often act as acceptor dopants in ferroelectric materials with a perovskite structure, for the variation in valencies from +4 to +2 and +3 at high temperatures.[7,8] In this process, oxygen vacancies appear as a result of charge compensation, and then the electrical properties of the crystal are affected. The oxygen vacancies pin the domain walls, and the defect dipoles, *i.e.* $Mn''_{Ti} - V^{\cdot\cdot}_O$, align with spontaneous polarization in a domain, leading to a hardening effect. Hard ferroelectrics are characterized by low permittivity, low losses, low piezoelectric coefficient and high coercive field.[9] There are numerous studies that report the Mn doping effect on relaxor ferroelectrics, such as Mn-doped PMN-PT, PIN–PMN–PT ceramics and single crystals.[10–13] It has been reported that doping Mn in relaxor-PT ferroelectrics could improve their electromechanical quality factor, thermal stability and pyroelectricity.[5,6,14] For example, the mechanical quality factor of PIN–PMN–PT (~100) can be improved through modification by Mn-doping to above 1000, which is comparable to that of hard PZT8 ceramics.[15]

As a member of relaxor ferroelectrics, $(1-x)Pb(In_{0.5}Nb_{0.5})O_3$–$xPbTiO_3$ (PIN–PT), with a composition near the morphotropic phase boundary (MPB), shows excellent properties such as high piezoelectric coefficient ($d_{33} > 350$ pC N^{-1} for ceramics, $d_{33} > 1500$ pC N^{-1} for single crystals), high Curie temperature ($T_C \geq 250$ °C) and large electromechanical coupling properties ($k_p \geq 0.7$).[3,16,17] Compared with bulk ceramics and films, single crystals exhibit a much better piezoelectric coefficient, ferroelectricity and electromechanical properties due to their homogeneity of composition and structure; in other words, crystals reflect the intrinsic state of materials to some extent. For these reasons, the Mn-doped PIN–PT solid solutions in the form of single crystals are supposed to possess excellent electrical properties for high temperature and high power applications. In order to study the effect of Mn dopants on the structure and electrical properties of PIN–PT crystals, single crystals with

[a]*Key Laboratory of Optoelectronic Materials Chemistry and Physics, Fujian Institute of Research on the Structure of Matter, Chinese Academy of Sciences, Fujian, Fuzhou 350002, China. E-mail: hechao@fjirsm.ac.cn; lxf@fjirsm.ac.cn*
[b]*University of Chinese Academy of Sciences, Beijing, China*

a composition of $0.61Pb(In_{0.5}Nb_{0.5})O_3$–$0.39Pb(Ti_{0.9}Mn_{0.1})O_3$ were grown and investigated.

2. Experimental

The Mn-doped PIN–PT single crystals were grown by the conventional flux method. The starting chemicals, PbO (99.9%), In_2O_3 (99.9%), Nb_2O_5 (99.9%), TiO_2 (99.9%), MnO_2 (99.9%), were weighed according to the nominal stoichiometric composition of $0.61Pb(In_{0.5}Nb_{0.5})O_3$–$0.39Pb(Ti_{0.9}Mn_{0.1})O_3$. The mixture of PbO and B_2O_3 (99.9%) was used as flux. The mixture of weighed chemicals was loaded in a platinum crucible and then placed in a vertical tubular furnace. The growing process was similar to the ones described by He *et al.*[18] with the main difference being that the temperature range between crystallizing and growing was from 1000 °C to 925 °C in this study. Finally, the Mn doped PIN–PT crystals were obtained.

The actual composition of the grown Mn-doped PIN–PT crystals was examined by inductively coupled plasma atomic emission spectroscopy (ICP-AES, JY Ultima-2, France). The structural analysis and sample orientation were examined by an X-ray diffractometer (Rigaku, Miniflex 600, Japan) at room temperature. Rietveld analyses were performed on the XRD pattern that was collected over the 2θ range 5°–85° with a step of 0.01° and counting time of 2 s per step, using fullprof software. A plate shaped crystal was cut perpendicularly to the [001] direction and finely polished to obtain optical quality with a thickness of about 60 μm, and the sample was annealed at 500 °C to remove the surface stress. The symmetry of the as-grown crystal was determined by a polarized light microscope (PLM, LV100POL, Nikon, Japan) connected to a computer. The [001]-oriented samples were prepared, polished and coated with silver paste, as electrodes for electric measurements. The ferroelectric hysteresis loops were displayed by an aix-ACCTIF2000 analyzer combined with a high-voltage supply amplifier/controller (Trek, model 610E). The piezoelectric coefficient was measured using a quasi-static d_{33} meter (Institute of Acoustics, Chinese Academy of Sciences, model ZJ-4AN). The dielectric constant (ε') and loss tangent ($\tan\delta$) were determined by a computer-controlled Alpha-A broad band dielectric/impedance spectrometer (Novocontrol GmbH, Germany). The same setup was employed to measure the resonance frequency (f_r) and anti-resonance frequency (f_a) as a function of temperature of a bar sample. The longitudinal electromechanical coupling factors (k_{33}) were calculated based on the resonance and anti-resonance frequencies using the following formula:

$$k_{33}^2 = \frac{\pi}{2}\frac{f_r}{f_a}\cot\left(\frac{\pi}{2}\frac{f_r}{f_a}\right) \quad (1)$$

3. Results and discussion

Fig. 1a inset shows the photograph of the Mn-doped PIN–PT crystals with dark color composed of several quadrate crystals, with the dimension of the largest crystal being about 10 mm × 5 mm × 5 mm. The actual chemical composition of the crystal was determined to be $0.68Pb(In_{0.5}Nb_{0.5})O_3$–$0.32Pb(Ti_{0.92}Mn_{0.08})O_3$ (O_3 (abbreviated as Mn-PIN–PT hereafter) according to the data from ICP measurements. The effective segregation K_{eff} of Mn ions can be determined using the following formula:

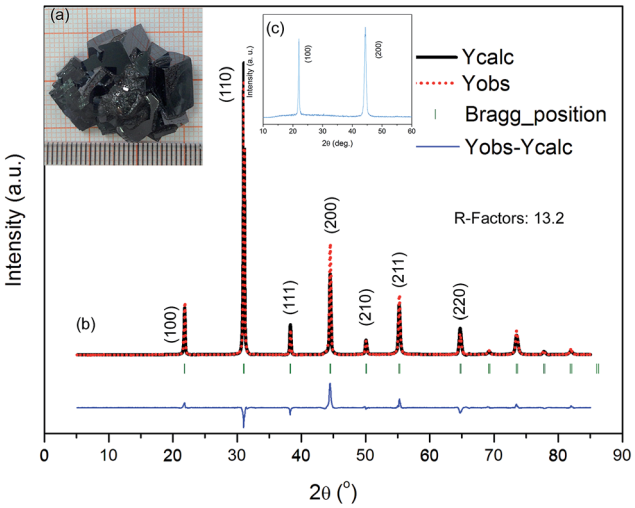

Fig. 1 (a) Photograph of the as-grown Mn-PIN–PT crystals; (b) Rietveld refinement of the XRD pattern of Mn-PIN–PT crystals; (c) XRD patterns of a platelet sample cut from the grown crystals, confirming the (001) plane.

$$K_{eff} = \frac{\left[\frac{C_{Mn}}{(C_{In}+C_{Nb}+C_{Ti}+C_{Mn})}\right]_C}{\left[\frac{C_{Mn}}{(C_{In}+C_{Nb}+C_{Ti}+C_{Mn})}\right]_S} \quad (2)$$

where the C_{Mn}, C_{In}, C_{Nb} and C_{Ti} are the concentrations of Mn, In, Nb and Ti in crystal (C) and solution (S), respectively, and the result was calculated to be 0.8. The XRD pattern of ground crystal powder is presented in Fig. 1b, showing a pure perovskite structure without any pyrochlore phase, which is consistent with pure PIN–PT single crystals with a similar composition, as shown in Table 1. In order to confirm the symmetry, a Rietveld refinement was carried out on the XRD data, as shown in Fig. 2c. The final refinement convergence was

Table 1 Comparison of ferroelectric, piezoelectric and dielectric properties of [001]-oriented Mn-doped and pure $(1-x)$PIN–xPT single crystals with similar compositions (FM: flux method; SBM: solution Bridgman method; TSSG: top-seed solution growth method; R: rhombohedral; PC: pseudo-cubic)

Materials	$x = 0.28$	$x = 0.34$	$x = 0.345$	$x = 0.32$
Growth method	FM	SBM	TSSG	FM
Phase symmetry	R	R	R	PC
T_m (°C)	260	265	290	231
T_{MPB} (°C)	100	134	150	175
P_r (μC cm^{-2})	—	26	30	25
E_C (kV cm^{-1})	—	6	9	9.7
ε	—	4100	1080	1284
$\tan\delta$ (%)	—	1.2	3	1
d_{33} (pC N^{-1})	700	2100	1600	730
Ref.	19	3 and 4	16	This work

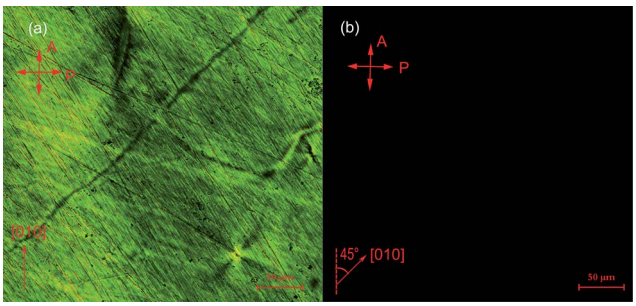

Fig. 2 Micrographs of [001]-oriented plate (60 μm thick) of as-grown Mn-PINT crystal at different positions under crossed polars (shown by arrows) at room temperature, showing rhombohedral crystallographic directions.

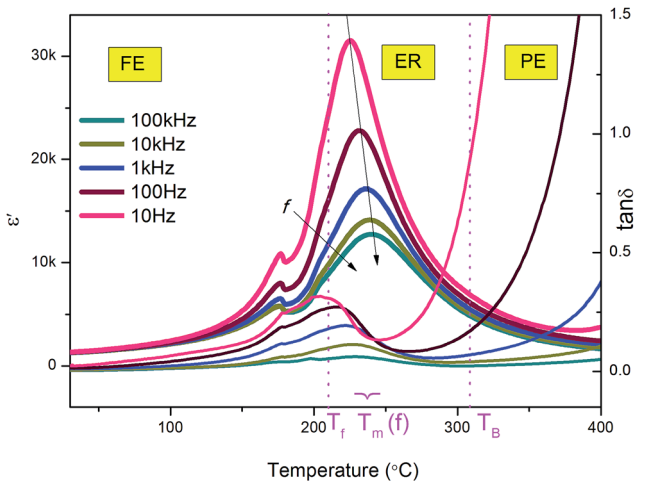

Fig. 3 Dielectric constant (ε') and loss tangent (tan δ) for the poled [001]-oriented Mn-PIN–PT single crystal as a function of temperature measured at various frequencies. T_f: freezing temperature, below which the PNRs are frozen and the ergodic state transforms to ferroelectric state; T_m: the temperature at which the dielectric permittivity reaches the maximum, varying with frequency in relaxors; T_B: Burns temperature, above which the relaxors obey the Curie–Weiss law.

Table 2 The radii of ions in the Mn-PIN–PT solid solutions (hs: high spin state)[36]

Ion	Pb	In	Nb	Ti	Mn		
Valence	+2	+3	+5	+4	+2	+3	+4
Coordination	XII	VI	VI	VI	VI	VI	VI
Ionic radius (Å)	1.49	0.8	0.64	0.67	0.83 (hs)	0.645 (hs)	0.53

achieved with R-factors = 13.2. The results show that the Mn-PIN–PT sample belongs to the $Pm\bar{3}m$ space group with a = 4.0713 Å, exhibiting a pseudo-cubic symmetry. The lattice parameters are larger than a = 4.0634 Å of 0.66PIN–0.34PT single crystals in ref. 3 and a = 4.064 of 0.72PIN–0.28PT in ref. 19. The expansion of lattice parameters may be caused by the variation of ionic radii. According to the spectrochemical series, the Mn^{2+}/Mn^{3+} would adopt a high spin state for the weak crystal field of O^{2-} ligands,[20,21] and the ionic radii have been listed in Table 2. Given that the ionic radius of Mn^{2+} is much larger than that of Ti^{4+}, the substitution of Mn for Ti in the lattice would inevitably lead to the increase of lattice parameters. The theoretical density of as-grown single crystals is 8.383 g cm^{-3} based on the lattice parameter. The XRD pattern for the facet of a tablet sample, which was cut from the as-grown crystals for electrical measurements, is shown in the Fig. 1c inset. The [001] oriented facet can be confirmed because only (001) and (002) reflection peaks appeared.

Fig. 2 shows the micrographs of the [001]-oriented crystal under a crossed polarizer at room temperature. The direction of spontaneous polarization, which is the vibration direction of the domain, is along the [111] directions in a rhombohedral/pseudo-cubic perovskite. Viewed under crossed polarizers, the domains appear to be in extinction when their slow and fast vibration directions are along the vibration directions of polarizer (P) and analyzer (A), and the extinction angle θ is defined as the smaller angle between the [100] or [010] crystallographic axis and the polarizer (P) or analyzer (A). In the case of [001]-oriented samples with pseudo-cubic symmetry, the extinction angle is practically 45° without exception, as shown in Fig. 2b. Rotating the sample, the vision would turn bright and reach full brightness at $\theta = 0°$, just as shown in Fig. 2a. Moreover, the field of view is dark at any angle for a cubic structure, thus confirming a pseudo-cubic symmetry.

The dielectric constant (ε') and loss tangent (tan δ) as a function of temperature at various frequencies for the poled [001]-oriented Mn-PIN–PT single crystal are shown in Fig. 3. The curve of dielectric constant *vs.* temperature shows a sharp peak at 231 °C (1 kHz), corresponding to the Curie temperature (T_C). Moreover, the minor peak at 175 °C corresponds to the temperature of phase transition from pseudo-cubic to tetragonal, represented as T_{MPB}. The dielectric constant and loss tangent at 1 kHz for the sample are 1284 and 0.01 at room temperature, respectively. In addition, it can be seen that T_m (the temperature where ε' shows a maximum) shifts slightly to a higher temperature as frequency increases, showing frequency dispersion, which is a feature of relaxor behavior. For normal ferroelectrics, the dielectric constant can be fitted by the Curie–Weiss law at a temperature higher than the Curie temperature:

$$\frac{1}{\varepsilon'} = \frac{T - T_{CW}}{C} \quad (3)$$

where C is the Curie constant, and T_{CW} is the Curie–Weiss temperature.[22] However, for relaxor ferroelectrics, ε' does not obey the Curie–Weiss above T_m until the Burns temperature (T_B) is reached, as shown in Fig. 4 by the dashed line. The Curie constant, T_B and Curie–Weiss temperature (T_{CW}) are determined from fitting with the value of 3.6 × 10^5, 309 °C and 254 °C, respectively. The diffusivity γ, which varies from 1 to 2 for normal and relaxor ferroelectrics, was calculated to be 1.63 according to the modified Curie–Weiss law,[23] confirming a certain degree of relaxor behavior. The dielectric constant

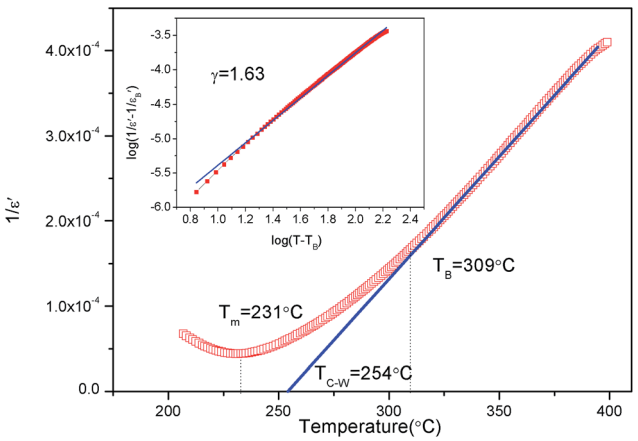

Fig. 4 Temperature dependence of $1/\varepsilon'$ at 1 kHz for the Mn-PIN–PT single crystal, the data above TB obeys the Curie–Weiss law. The inset shows the $\log(1/\varepsilon' - 1/\varepsilon'_B)$ *vs.* $\log(T - T_B)$ curve for estimation of diffuseness component γ.

deviation from Curie–Weiss is caused by the formation of local polar nanoregions (PNRs).[22,24] At a temperature higher than the Burns temperature, the Curie–Weiss law is obeyed well as mentioned previously. At the Burns temperature, the PNRs emerge, and their coupling is forbidden by thermal fluctuation until the temperature drops to T_{CW}. As the temperature decreases, the volume fraction of the polar region increases and the thermal disordering effect decreases, causing the onset of correlation. On cooling to a certain temperature, the polarization fluctuation will be frozen and normal ferroelectrics will be developed, and eventually almost all of the PNRs will be frozen. This temperature is defined as freezing temperature (T_f), and its location is marked in Fig. 3. It can be seen that the freezing temperature separates the ferroelectric state at a low temperature and the ergodic state at a high temperature.

The ferroelectric hysteresis loops of the [001]-oriented Mn-PIN–PT single crystals were measured at various electric fields (f = 10 Hz) at room temperature, and the result is shown in Fig. 5. It is clear that the polarization is saturated above an electric field of 30 kV cm^{-1}, and the remnant polarization P_r and coercive field E_C (at the electric field of 30 kV cm^{-1}), at room temperature, are 25 μC cm^{-2} and 9.7 kV cm^{-1}, respectively. As a result of internal bias field E_i, the hysteresis loops exhibit evident asymmetric features.

Fig. 6a shows that the ferroelectric hysteresis loops were measured at temperatures varying from room temperature to 285 °C, to investigate the temperature stability of the PIN–PT crystals with Mn doping. The temperature dependence of remnant polarization P_r, coercive field E_C and internal bias field E_i were plotted for better analysis, as shown in Fig. 6b. The values of E_C and E_i were determined, respectively, using the following formula:

$$E_C = \frac{E_C^+ - E_C^-}{2}, \quad E_i = \frac{E_C^+ + E_C^-}{2} \tag{4}$$

where E_C^+ and E_C^- are the intersections of the hysteresis loops with abscissa axis in the positive and negative directions, respectively. The abnormal increase of remnant polarization in

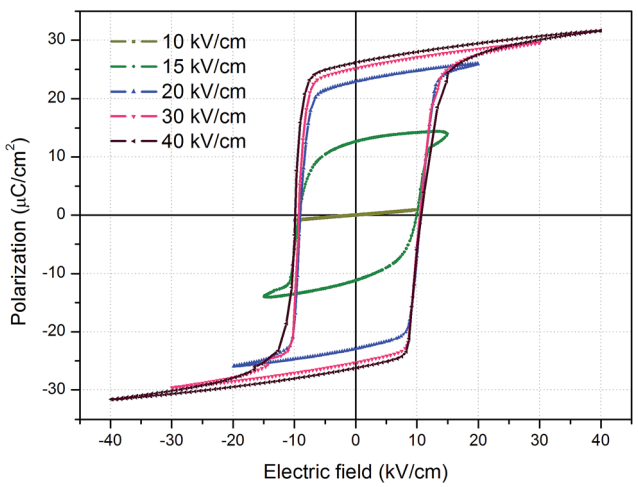

Fig. 5 Ferroelectric hysteresis loops for the [001]-oriented Mn-PIN–PT single crystal measured at different electric fields at room temperature (at 10 Hz).

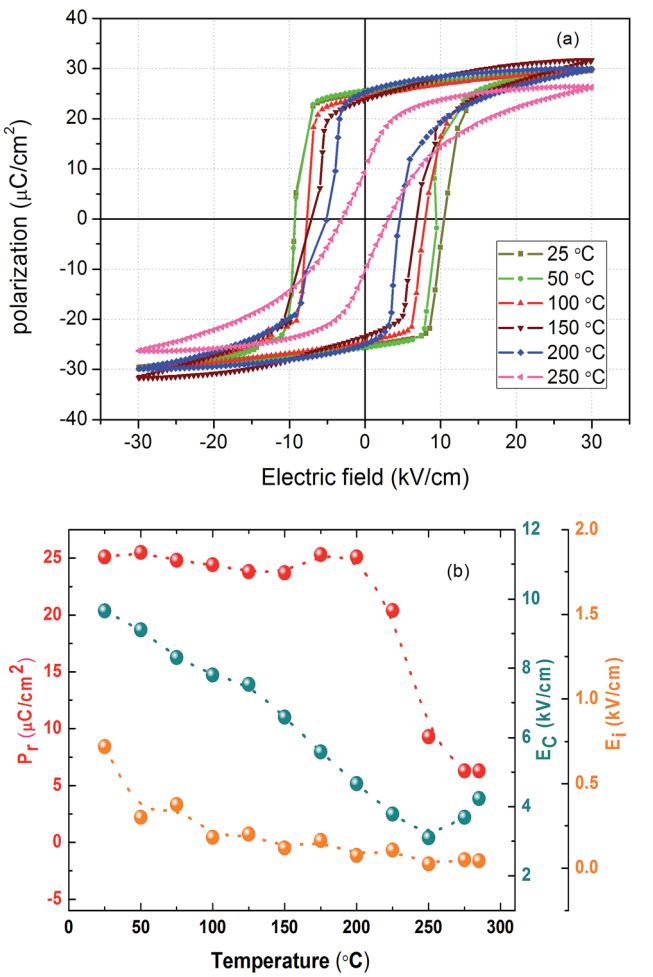

Fig. 6 Temperature dependence of (a) ferroelectric hysteresis loops, (b) remnant polarization (Pr), coercive field (EC) and internal bias field (E_i) for the Mn-PIN–PT single crystal (10 Hz).

the vicinity of 160 °C is mainly caused by the ferroelectric phase transition.[25] The remnant polarization remains almost the same before T_{MPB} and then decreases continuously, thus providing the potential for application in the high temperature field. Moreover, the coercive field decreases linearly as the temperature increases to T_C. However, the values of P_r and E_C do not decrease to zero immediately above the Curie temperature, which happens in normal ferroelectric materials; the residual $P_r \sim 6.3\ \mu C\ cm^{-2}$ and $E_C \sim 4\ kV\ cm^{-1}$ subsist up to 285 °C. This type of behavior is similar to relaxor ferroelectrics, in which a macro polarization can be induced.[26] This result confirms a certain degree of relaxor behavior in the Mn-PIN–PT single crystal, which is in agreement with the dielectric analysis.

As a result of the hardening effect, the value of the piezoelectric coefficient at room temperature was measured to be 730 pC N^{-1}, which is inferior compared with that of pure PIN–PT single crystals, *i.e.*, the d_{33} of PIN–PT (65.5/34.5) single crystals grown *via* the TSSG method is 1600 pC N^{-1}.[16] To study the electromechanical coupling properties of the crystal, the resonance (f_r) and anti-resonance frequencies (f_a) of a bar sample with a size of 2.36 × 3.12 × 6.22 mm^3 were measured at room temperature. The frequency dependence of impedance and phase angle are shown in the inset of Fig. 7. Two peaks at 172 000 and 272 000 Hz correspond to the resonance frequency (f_r) and anti-resonance frequency (f_a), respectively, and the electromechanical coupling factor (k_{33}) is calculated to be 80% according to formula (1). The electromechanical coupling factor (k_{33}) of the [001]-oriented Mn-PIN–PT crystal as a function of temperature was investigated and is shown in Fig. 7. It can be seen that the temperature coefficient of k_{33} is calculated to be 1.6% with a temperature increase to 180 °C, indicating good temperature stability, which is beneficial for application in this temperature range.

To study the influence of Mn doping on the properties of the PIN–PT single crystals, the parameters of ferroelectric, piezoelectric and dielectric properties for pure and Mn-doped PIN–PT single crystals with similar content of PT are listed in Table 2. For most relaxor-PT solid solutions with compositions located on the same side of the MPB region, the properties vary continuously with the increase in PT content, with certain rules.[27,28] Thus, the properties of 0.68PIN–0.32PT single crystals can be estimated through the parameters of samples with similar compositions. It can be seen that when Mn was doped, the Curie temperature of PIN–PT single crystals decreased by about 30 °C; however, the T_{MPB} increased by approximately 50 °C. In order to explain the decrease of T_C, the oxygen vacancies should be taken into consideration. It is well known that the substitution of an ion with a lower valence state (Mn^{2+}/Mn^{3+} for Ti^{4+} in this case) in the lattice would lead to the appearance of oxygen vacancies for charge compensation. Moreover, the oxygen vacancies introduced by acceptor dopants are intrinsic defects, which cannot be eliminated by annealing.[8] Thus, the Curie temperature would decrease because of the stabilization of the cubic phase, which is a consequence of both the presence of oxygen vacancies and the acceptor dopants (Mn^{2+} and Mn^{3+}), in which the type of electronic ground state is the main factor that essentially matters.[8,29] However, it should be noted that in ref. 10, the T_{MPB} of the samples decreases as Mn is doped in, which is in contradiction with the results of this study. The substitution of Mn^{2+}/Mn^{3+} for Ti^{4+} in the B site of the perovskite and the presence of oxygen vacancies could reduce the *c*/*a* ratio and decrease the tetragonality of the crystals,[20,30] thus possibly stabilizing the pseudo-cubic structure and leading to an increment in the temperature of phase transition from pseudo-cubic to tetragonal. The dielectric response and dielectric loss are both suppressed by the defect dipoles through pinning the domain walls, leading to the decrease of dielectric constant and dielectric loss.[6,31]

The effect of Mn doping on the ferroelectric property is exhibited numerically by the changes of remnant polarization, coercive field and internal bias field. A slight decrease of P_r and increase of E_C can be observed in Table 2. This variation is a typical feature of the hardening effect, which is caused by acceptor doping.[5] According to the principle of symmetry-conforming short-range order (SC-SRO), the defect dipoles formed between Mn^{2+}/Mn^{3+} ions and oxygen vacancies produce a defect polarization P_D that is in the same direction with spontaneous polarization P_S within each domain, leading to an internal bias field that provides a driving force for domain stability and hinders domain wall mobility.[32,33] As a result, the stability of the ferroelectric domains is enhanced by the internal bias field, the remnant polarization decreases and the coercive field increases for the Mn-doped PIN–PT single crystals. At the same time, the piezoelectric coefficient decreases at the expense of the increment of the coercive field. At elevated temperatures, the symmetry configuration of defect dipoles will be changed by the migration of oxygen vacancies. When temperature increases, the induced higher thermal fluctuation decreases the activation energy for diffusion of oxygen vacancies and relieves the resistance for domain switching.[34,35] As a consequence, the internal bias field E_i decreases significantly with increasing temperature, as shown in Fig. 6.

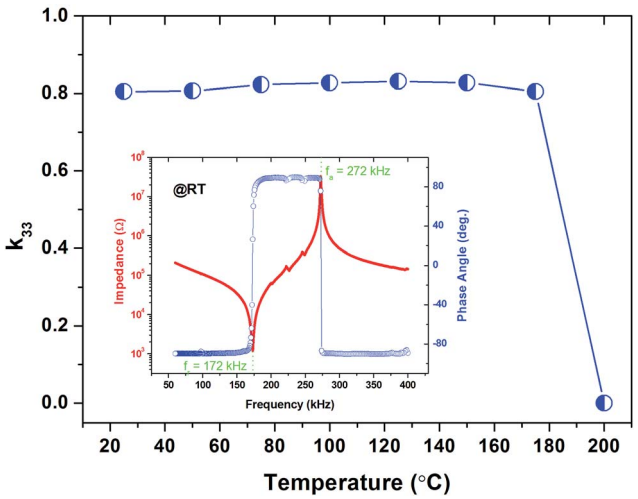

Fig. 7 k_{33} as a function of temperature for the [001]-oriented Mn-PINT single crystals. The inset shows the impedance and phase angle as a function of frequency at room temperature. The solid lines are guides for the eyes based on the measured data shown by dots.

4. Conclusion

In summary, the binary Mn-PIN–PT ferroelectric single crystals with perovskite structure, exhibiting [001]-oriented natural facets, were grown successfully *via* the flux method. The characteristics of the structure, dielectric and ferroelectric properties for the [001]-oriented single crystals have been investigated. The Curie temperature and ferroelectric phase transition temperature were detected to be 231 °C and 175 °C, respectively. The dielectric constant and loss tangent at room temperature (1 kHz) are 1284 and 0.01 for a poled [001]-oriented single crystal. At an electric field of 30 kV cm^{-1}, the remnant polarization and coercive field at room temperature are 25 μC cm^{-2} and 9.7 kV cm^{-1}, respectively. Compared with pure PIN–PT single crystals, the Mn-doped samples possess a higher Curie temperature and lower T_{MPB} as a consequence of internal bias field and reduction of tetragonality. The piezoelectric coefficient (d_{33}) and longitudinal electromechanical coupling factor (k_{33}) are 730 pC N^{-1} and 80% at room temperature, respectively. Particularly, the temperature dependence of k_{33} exhibits good stability with the temperature coefficient of 1.6% below 180 °C. The defect polarization P_D was formed between Mn and oxygen vacancies, exhibiting an internal bias field. Then, the hardening effect is formed because of the internal bias field, which can pin the domain walls and provide a driving force for domain stability. Therefore, the coercive field increases, and the remnant polarization, piezoelectric coefficient, dielectric constant and dielectric loss decrease for the hardening effect of the acceptor dopants.

Acknowledgements

This study was supported by the National Natural Science Foundation of China (Grant No. 11404331, 91422303, 11504373, 51602308), the Strategic Priority Research Program of the Chinese Academy of Sciences (Grant No. XDB20000000) and "Chunmiao" Talents Program for Young Scientists of Haixi Institute of the Chinese Academy of Sciences (CMZX-2016-006).

References

1 M. Kobayashi, C. K. Jen, J. F. Bussiere and K. T. Wu, *NDT&E Int.*, 2009, **42**, 157–161.
2 I. El-Kady, R. H. Olsson and J. G. Fleming, *Appl. Phys. Lett.*, 2008, **92**, 3.
3 Z. Q. Duan, G. S. Xu, X. F. Wang, D. F. Yang, X. M. Pan and P. C. Wang, *Solid State Commun.*, 2005, **134**, 559–563.
4 Y. P. Guo, H. S. Luo, T. H. He, X. M. Pan and Z. W. Yin, *Mater. Res. Bull.*, 2003, **38**, 857–864.
5 E. W. Sun and W. W. Cao, *Prog. Mater. Sci.*, 2014, **65**, 124–210.
6 Y. Tang, L. Luo, Y. Jia, H. Luo, X. Zhao, H. Xu, D. Lin, J. Sun, X. Meng and J. Zhu, *Appl. Phys. Lett.*, 2006, **89**, 162906.
7 L. X. He and C. E. Li, *J. Mater. Sci.*, 2000, **35**, 2477–2480.
8 P. Hansen, D. Hennings and H. Schreinemacher, *J. Electroceram.*, 1998, **2**, 85–94.
9 J. F. Tressler, S. Alkoy and R. E. Newnham, *J. Electroceram.*, 1998, **2**, 257–272.
10 Z. Ren and Z. G. Ye, *Ferroelectrics*, 2014, **464**, 130–135.
11 L. H. Luo, D. Zhou, Y. X. Tang, Y. M. Jia, H. Q. Xu and H. S. Luo, *Appl. Phys. Lett.*, 2007, **90**, 3.
12 J. H. Park, J. Park, J. G. Park, B. K. Kim and Y. Kim, *J. Eur. Ceram. Soc.*, 2001, **21**, 1383–1386.
13 X. Q. Huo, S. J. Zhang, G. Liu, R. Zhang, J. Luo, R. Sahul, W. W. Cao and T. R. Shrout, *J. Appl. Phys.*, 2012, **112**, 5.
14 Y. Wang, E. Sun, W. Song, W. Li, R. Zhang and W. Cao, *J. Alloys Compd.*, 2014, **601**, 154–157.
15 L. M. Zheng, R. Sahul, S. J. Zhang, W. H. Jiang, S. Y. Li and W. W. Cao, *J. Appl. Phys.*, 2013, **114**, 6.
16 C. He, X. Z. Li, Z. J. Wang, Y. Liu, D. Q. Shen, T. Li and X. F. Long, *J. Alloys Compd.*, 2012, **539**, 17–20.
17 A. Kirianov, N. Ozaki, H. Ohsato, N. Kohzu and H. Kishi, *Jpn. J. Appl. Phys., Part 1*, 2001, **40**, 5619–5623.
18 C. He, X. Z. Li, Z. J. Wang, Y. Liu, D. Q. Shen, T. Li, X. F. Long and Z. G. Ye, *CrystEngComm*, 2012, **14**, 4407–4413.
19 N. Yasuda, H. Ohwa, M. Kume, K. Hayashi, Y. Hosono and Y. Yamashita, *J. Cryst. Growth*, 2001, **229**, 299–304.
20 Y. D. Hou, M. K. Zhu, F. Gao, H. Wang, B. Wang, H. Yan and C. S. Tian, *J. Am. Ceram. Soc.*, 2004, **87**, 847–850.
21 S. T. K. Toshio, T. Takaaki and D. Masaki, *Jpn. J. Appl. Phys.*, 1992, **31**, 3.
22 D. Viehland, S. J. Jang, L. E. Cross and M. Wuttig, *Phys. Rev. B: Condens. Matter Mater. Phys.*, 1992, **46**, 8003–8006.
23 T. Li and X. F. Long, *Mater. Res. Bull.*, 2014, **51**, 251–257.
24 R. A. Cowley, S. N. Gvasaliya, S. G. Lushnikov, B. Roessli and G. M. Rotaru, *Adv. Phys.*, 2011, **60**, 229–327.
25 Z. Li, Z. Xi, Z. Xu and X. Yao, *J. Mater. Sci. Lett.*, 2002, **21**, 1325–1327.
26 L. E. Cross, *Ferroelectrics*, 1987, **76**, 241–267.
27 X. F. Long and Z. G. Ye, *Chem. Mater.*, 2007, **19**, 1285–1289.
28 S. Wongsaenmai, X. L. Tan, S. Ananta and R. Yimnirun, *J. Alloys Compd.*, 2008, **454**, 331–339.
29 H. J. Hagemann and H. Ihrig, *Phys. Rev. B: Condens. Matter Mater. Phys.*, 1979, **20**, 3871–3878.
30 H. Qiao, C. He, Z. Wang, X. Li, Y. Liu, X. Yang, H. Tailor and X. Long, *Mater. Des.*, 2017, **117**, 232–238.
31 E. W. Sun, R. Zhang, F. M. Wu, B. Yang and W. W. Cao, *J. Appl. Phys.*, 2013, **113**, 4.
32 X. B. Ren, *Nat. Mater.*, 2004, **3**, 91–94.
33 L. X. Zhang and X. B. Ren, *Phys. Rev. B: Condens. Matter Mater. Phys.*, 2006, **73**, 6.
34 G. S. Xu, H. S. Luo, H. Q. Xu, Z. Y. Qi, P. C. Wang, W. H. Zhong and Z. W. Yin, *J. Cryst. Growth*, 2001, **222**, 202–208.
35 G. Du, R. H. Liang, L. Wang, K. Li, W. B. Zhang, G. S. Wang and X. L. Dong, *Appl. Phys. Lett.*, 2013, **102**, 4.
36 Database of Ionic Radii, http://abulafia.mt.ic.ac.uk/shannon/ptable.php.

